ELSEVIER

Bioelectrochemistry 58 (2002) 171–180

Bioelectrochemistry

www.elsevier.com/locate/bioelechem

The complex dielectric spectrum of heart tissue during ischemia

M. Schaefer *, W. Gross, J. Ackemann, M.M. Gebhard

Department of Experimental Surgery, University of Heidelberg, INF 365, D-69120 Heidelberg, Germany

Received 8 March 2002; received in revised form 2 August 2002; accepted 5 August 2002

Abstract

Introduction: Because of the variety of tissue structures, the interpretation of the passive complex dielectric permittivity spectrum $\varepsilon(\omega)$ of the heart is still a problem. The aim of this work was to correlate $\varepsilon(\omega)$ of heart tissue with physical processes on cellular level. *Methods*: $\varepsilon(\omega)$ of canine hearts was continuously measured in the range from 10 Hz to 400 MHz during cardioplegic perfusion and during following ischemia. Cardioplegic perfusion was performed with HTK (Custodiol®) without or with heptanol, in order to produce electrical cell uncoupling via the closure of gap junctions. To analyse $\varepsilon(\omega)$, we present two heart models which consider cell shape, electrical cell coupling, and dielectric polarisation of cell membranes and membranes of intracellular structures. *Results*: $\varepsilon(\omega)$ of heart tissue shows an α-, β-, and γ-dispersion. $\varepsilon(\omega)$ remains unchanged during cardioplegic perfusion with HTK, but if heptanol is added, there is an immediate decrease in the region of α-dispersion and an increase in the low frequency part of β-dispersion. Similar changes are observed during ischemia following HTK perfusion without heptanol; additionally, the β-dispersion shifts to higher frequencies. Using our models, we obtain analogue changes of $\varepsilon(\omega)$ by fitting model parameters which describe water content, water distribution, extra- and intracellular conductivity, and gap junction resistance. *Discussion*: Changes of these tissue properties as calculated by our models based on the measurement of $\varepsilon(\omega)$ are consistent with intraischemic changes of heart tissue known from immunohistochemical, biochemical, and histological investigations. The next step will be to use our models for the prognosis of irreversible tissue damage.

Keywords: Dielectric spectroscopy; Heart; Ischemia; Tissue models; Water content; Gap junctions

1. Introduction

The dielectric polarisation of matter is given by the dimensionless parameter ε', which is called dielectric permittivity [1]. ε' describes the capacitance increase of a capacitor filled with matter:

$$\varepsilon' = \frac{C}{C_0} \tag{1}$$

with C = capacitor with matter, C_0 = vacuum capacitor.

Typically, the dielectric polarisation processes are frequency-dependent and show relaxation phenomena with increasing frequency. The relaxation processes are described by the complex dielectric permittivity ε in Eq. (2):

$$\varepsilon(\omega) = \varepsilon'(\omega) - i\varepsilon''(\omega) \tag{2}$$

with ε' = dielectric permittivity, ε'' = dielectric loss factor, $\omega = 2\pi f$, f = frequency, and i = imaginary unit $(= \sqrt{-1})$.

The dielectric losses are usually described by the frequency-dependent conductivity $\sigma(\omega)$ of the matter (Eq. (3)),

$$\sigma(\omega) = \omega\varepsilon_0\varepsilon''(\omega) \tag{3}$$

with $\varepsilon_0 = 8.85 \times 10^{-12}$ As/Vm.

From relaxation phenomena in the dielectric spectra, one can gain information about molecular dipole moments [2], chemical interactions between different molecules [3], cellular membranes and structures [4–6], subcellular structures like mitochondria [7,8], and many other dynamic processes like counter ion polarisation [5].

The dielectric polarisation of matter can be measured nondestructively by the application of weak electric fields [1,6]. Therefore, the method of dielectric spectroscopy seems to be a suitable means for noninvasive investigations on living tissue. A large growing body of literature exists dealing with measuring the impedance or the dielectric spectra of various biological tissues in the frequency range from DC up to several GHz [9–12].

One field of application of this spectroscopy technique is the characterisation of heart tissue during global ischemia [13–16]. During ischemia, the blood flow through the heart

* Corresponding author. Tel.: +49-6221-561755; fax: +49-6221-564208.

E-mail address: michael.schaefer@exchi.uni-heidelberg.de (M. Schaefer).

1567-5394/02/$ - see front matter © 2002 Elsevier Science B.V. All rights reserved.
PII: S1567-5394(02)00152-4

is interrupted and the tissue undergoes progressive changes leading to irreversible loss of its viability. These progressive changes seem to be correlated to changes in the passive electrical impedance spectrum of the heart measured during ischemia [13,16]. However, interpretation of the spectrum of the heart and its changes during ischemia is still difficult. The reason for this is the complex structure of heart tissue. Many of the above-mentioned polarisation mechanisms contribute to its dielectric permittivity and the relaxation processes overlap each other in the spectrum. A clear correlation between a measured intraischemic alteration in the dielectric spectrum and a physical process on the cellular level was not yet found and the interpretation strongly depends on the chosen model [13,14]. One new aspect of discussion is the closure of gap junction channels which connect heart cells electrically. The intraischemic variation of intercellular coupling is assumed to be one possible reason for some of the measured changes of the dielectric spectrum [14,17–19]. The open state of these gap junctions is suspected to take part in cardiac diseases especially concerning arrhythmogenesis and cardiac contractile dysfunction [18,20–23]. Patch clamp techniques on paired cells, immunohistochemical methods, laser scanning microscopy or electron microscopy are mostly used for the investigations of the gap junctions [24]. In comparison to these techniques, dielectric spectroscopy is noninvasive and very simple to use. However, the previous studies show [14,17,18] that the information about electrical cell coupling from complex impedance spectra are very vulnerable to disturbances produced by temperature, conductivity of the extracellular fluid, and electrode position. Therefore, absolute measurements are difficult and information was obtained only by analysing the time course relative to the starting values.

The aim of this work was to correlate the complex dielectric permittivity spectrum of the heart measured from 10 Hz to 400 MHz with physical processes on cellular level. We discuss the measurements in the scope of two different heart models. The first heart model was suggested by Gersing [14] for liver tissue and is modified in this work for the application on heart. It describes the electrical properties of different tissue structures by using a network of technical components. However, this model does not allow for the distribution of time constants [25–27] or the influence of cell shapes [28]. In order to consider also these phenomena, we present a second heart model which includes the knowledge about tissue morphology and the dielectric properties of the different tissue materials. With these models, we try to answer the following questions:

(1) Can we identify the open state of gap junctions by using the technique of complex dielectric spectroscopy? For this purpose, we measured the complex dielectric permittivity spectrum of heart tissue during cardioplegic perfusion and following ischemia in two different situations: perfusion with HTK (Custodiol®) as in the hospital situation and perfusion with HTK + 3 mmol/l heptanol in order to close the gap junctions [29].
(2) Is it possible to correlate intraischemic processes known from biochemical and histological investigations with changes in the dielectric spectrum? For this purpose, we fitted a heart model to the dielectric measurements and compared the tissue properties described by the model parameters with intraischemic processes known from biochemical and histological investigations.
(3) What is the influence of cell shape and the shapes of intracellular structures on the tissue water content determined by dielectric spectroscopy? For this purpose, we calculated the effective dielectric permittivity produced by the dipole moments of water molecules with the second model. The result is used for the determination of the tissue water content from dielectric permittivity measurements which is compared to the water content gained by drying and weighing heart tissue samples.
(4) Is it possible to assess tissue damage in ischemic hearts by means of dielectric spectroscopy?

2. Materials and methods

2.1. Experimental procedure

All animals received humane care according to the Guide for the Care and Use of Laboratory Animals (NIH, pub. 86-23, revised 1985).

After anaesthesia and thoracotomy, the left ventricular myocardium of dogs (Foxhounds) was investigated during cardioplegic perfusion with 5 °C cold HTK (Köhler Chemie, Alsbach-Hähnlein, Germany) or with the intermixture of 3 mmol/l heptanol. HTK group consisted of $n = 6$ dogs and the effect of heptanol was tested in $n = 5$ experiments. Both groups were further investigated during following ischemia at 25 °C [13].

After the first 2 min of cardioplegic perfusion with HTK, heartbeat had stopped. Then, the probe for dielectric measurements was smoothly pressed to the epicardial surface of the left ventricle and the complex dielectric spectrum was measured continuously every minute. Perfusion with HTK was continued up to 11 min. Alternatively, heptanol was injected in the fifth min of perfusion into the HTK solution and perfusion was also continued up to 11 min. After the end of perfusion, pieces of 2.5 × 2.5 cm were excised from the left ventricle and placed in temperature-controlled measuring chambers at 25 °C for the dielectric measurements during ischemia [30]. No bath medium was added but chambers were sealed to avoid desiccation. The complex dielectric permittivity spectrum was measured during ischemia continuously every 10 min.

One piece of each left ventricle was weighed and dried in order to determine the dry-to-wet weight ratio of the heart tissue. Water content was also determined in pieces of left

ventricle tissue after 20 min of heart perfusion with saline solution ($n = 15$).

2.2. The dielectric spectrum from 10 Hz to 10 MHz

The dielectric permittivity spectrum $\varepsilon(\omega)$ was measured by using an impedance spectroscopy equipment consisting of a computer controlled Solartron 1260 impedance analyser together with a self-constructed preamplifier [31] and non-invasive surface electrodes. The electrode probe consisted of two electrodes arranged in parallel with a distance of 10 mm between them [30]. Each electrode had a fractal surface in order to minimise electrode polarisation errors and an area of 4×1 mm.

The dielectric permittivity $\varepsilon(\omega)$ was calculated from the measured complex impedance $Z(\omega)$ by Eq. (4).

$$\varepsilon(\omega) = \frac{1}{i\omega\ C_0 Z(\omega)} \tag{4}$$

The impedance $Z(\omega)$ is altered by the impedance of the electrical network connecting the electrode probe and the measuring input. Eq. (5) gives the relation between the sample impedance $Z(\omega)$ and the measured impedance $Z_m(\omega)$ [6,32]:

$$Z_m(\omega) = W_{11}(\omega) + \frac{W_{12}(\omega)W_{21}(\omega)}{Z(\omega) - W_{22}(\omega)} \tag{5}$$

System calibration was performed by using three different saline solutions (KCl) with known dielectric properties for the determination of the scattering matrix parameter $W_{11}(\omega)$, $W_{12}(\omega)W_{21}(\omega)$, and $W_{22}(\omega)$.

2.3. The dielectric spectrum from 10 to 400 MHz

The complex reflection coefficient $r(\varepsilon,\omega)$ was measured with a Philips PM 5390 S signal generator and a Rhode and Schwarz ZPV-E3 HF analyser applying an open-ended coaxial line probe. The diameter of the outer conductor of the probe was 13 mm.

The quasi-static approximation of the complex admittance $Y(\varepsilon)$ of the coaxial line probe [33] was used to calculate the dielectric permittivity $\varepsilon(\omega)$ from Eq. (6).

$$r(\varepsilon,\omega) = \frac{Y_L - Y(\varepsilon)}{Y_L + Y(\varepsilon)} \tag{6}$$

with Y_L = admittance of the coaxial line.

The connecting electrical network between the probe and the measuring input changes the reflection coefficient $r(\varepsilon,\omega)$ to $r_m(\varepsilon,\omega)$ similar to the transformation of $Z(\omega)$ to $Z_m(\omega)$ in Eq. (5). For system calibration, air, shorted electrodes, and a saline solution (KCl) with known dielectric properties were used.

2.4. The equivalent circuit model of the heart

Fig. 1 shows the technical model suggested by Gersing for liver tissue [14] modified for application on heart tissue. This model describes the current through the tissue by using technical components in order to simulate the electrical properties of biological structures. The resistance R_e describes the properties of the extracellular electrolyte and the resistance R_i, the intracellular cytosol. This model bases on the vision that the transcellular current has to pass the membrane with the capacitance C_m and the resistance R_m, then through the cytosol, and from cell to cell through the interstitial membranes described by C'_m, or alternatively, through the gap junctions with the resistance R_{cc}.

2.5. The heart model based on tissue morphology

With regard to calculations of the dielectric spectrum in the broad frequency range from 10 Hz to 400 MHz, the frequency-dependent polarisation of various molecules, the Maxwell–Wagner polarisation of cell membranes as well as the polarisation contribution of intracellular structures like mitochondria have to be considered in the model [5,8,34]. Fig. 2 shows our simplified tissue model of the heart which we used for the calculations. The model consists of three compartments filled with different dielectric materials: the extracellular volume V_e ($\varepsilon_e(\omega)$), intracellular volume V_{ia} ($\varepsilon_{ia}(\omega)$), and the internal volume of subcellular structures like mitochondria V_{ii} ($\varepsilon_{ii}(\omega)$). The three compartments are separated from each other by membranes with the dielectric properties $\varepsilon_m(\omega)$ or $\varepsilon_{mi}(\omega)$, respectively. The dielectric properties $\varepsilon_k(\omega)$, k = e, ia, ii, m,

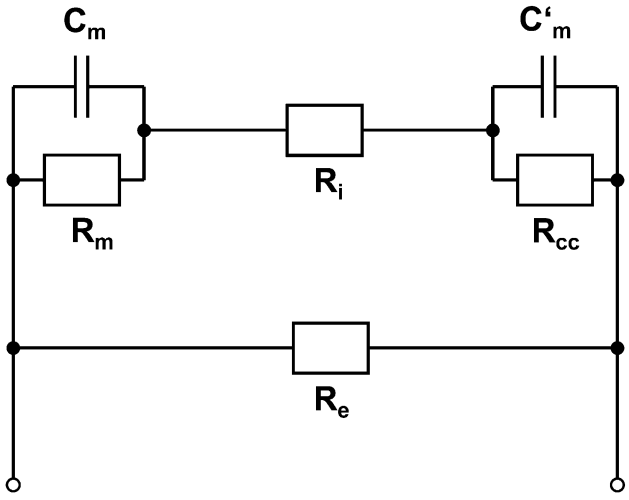

Fig. 1. Electrical model of organ tissue with intercellular connections via gap junctions suggested by Gersing [14] modified for the application on heart tissue by membrane resistance R_m. Membrane capacitance C_m, C'_m; cytosol resistance R_i; extracellular resistance R_e; and gap junction resistance R_{cc}.

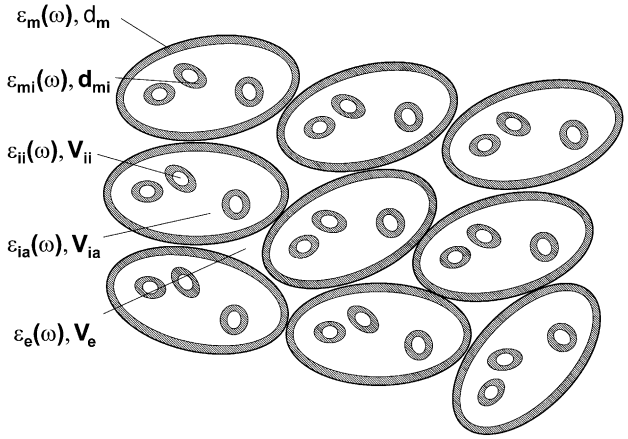

Fig. 2. Simplified model of heart tissue. The model consists of three compartments filled with different dielectric materials: the extracellular volume V_e ($\varepsilon_e(\omega)$), intracellular volume V_{ia} ($\varepsilon_{ia}(\omega)$), and the internal volume of subcellular structures like mitochondria V_{ii} ($\varepsilon_{ii}(\omega)$). The three compartments are separated from each other by membranes with the dielectric properties $\varepsilon_m(\omega)$ or $\varepsilon_{mi}(\omega)$, respectively. The dielectric properties $\varepsilon_k(\omega)$, k = e, ia, ii, m, mi, are calculated by using the Cole–Cole spectral function of Eq. (7).

mi, are calculated by using the Cole–Cole spectral function of Eq. (7) [35].

$$\varepsilon_k = \varepsilon_k(\infty) + \frac{\varepsilon_k(0) - \varepsilon_k(\infty)}{1 + (i\omega\tau_k)^{1-\alpha_k}} + \frac{\sigma_k}{i\varepsilon_0\omega} \tag{7}$$

with $\varepsilon_k(0)$ = static dielectric permittivity, $\varepsilon_k(\infty)$ = high frequency dielectric permittivity, τ_k = relaxation time, α_k = distribution parameter, and σ_k = DC conductivity.

The cell shape and the shape of the intracellular structures are approximated by rotational ellipsoids. The total dielectric permittivity $\varepsilon(\omega)$ of the model is obtained by two main steps.

(1) Computing the dielectric permittivity of the membrane enclosed ellipsoids of the intracellular structures by using Eq. (8) [36]:

$$\varepsilon_{2lj} = \varepsilon_3 \frac{\varepsilon_3 + (\varepsilon_2 - \varepsilon_3)D_{1lj} + \upsilon_l(\varepsilon_2 - \varepsilon_3)(1 - D_{0lj})}{\varepsilon_3 + (\varepsilon_2 - \varepsilon_3)D_{1lj} - \upsilon_l(\varepsilon_2 - \varepsilon_3)D_{0lj}}$$

$$D_{slj} = \frac{a_{isl}b_{isl}^2}{2}\int_0^\infty \frac{\mathrm{d}\xi}{(j^2 + \xi)\sqrt{(\xi + a_{isl}^2)(\xi + b_{isl}^2)^2}}$$

$$\upsilon_l = \frac{a_{i1l}b_{i1l}^2}{a_{i0l}b_{i0l}^2} \approx \frac{(a_{i0l} - d_{il})(b_{i0l} - d_{il})^2}{a_{i0l}b_{i0l}^2} \tag{8}$$

with $\varepsilon_2 = \varepsilon_{ii}(\omega)$, $\varepsilon_3 = \varepsilon_{mi}(\omega)$ calculated by Eq. (7), a, $b = c$ are the half axes of the ellipsoids, $j = a_{isl}$, b_{isl}, c_{isl}, $s = 0$ is used for the outer shape of the ellipsoid and $s = 1$ for the inner part of the ellipsoid without the membrane, d_{il} is the membrane thickness, and l is the index for the different shapes of the ellipsoids.

(2) Computing the effective dielectric permittivity ε_i of the inner compartment of the cell ellipsoids by using the mixture formula of Eq. (9) especially suitable for high volume fractions of the dissolved ellipsoidal component [37]:

$$\varepsilon_i - \varepsilon_1 = \frac{1}{3}\sum_l \upsilon_{il}\sum_j(\varepsilon_{2lj} - \varepsilon_1)\frac{\varepsilon_i}{\varepsilon_i + D_{0lj}(\varepsilon_{2lj} - \varepsilon_i)} \tag{9}$$

with $\varepsilon_1 = \varepsilon_{ia}(\omega)$ calculated by Eq. (7) and the volume fraction $\upsilon_{il} = V_{ii}/(V_e + V_{ia} + V_{ii})$.

Steps (1) and (2) are repeated for the ellipsoids describing the shape of the heart cells and the effective dielectric permittivity ε_{th} of the model tissue is calculated by using $\varepsilon_2 = \varepsilon_i(\omega)$, $\varepsilon_3 = \varepsilon_m(\omega)$, $\varepsilon_1 = \varepsilon_e(\omega)$, $d_{il} = d_m$, and $\upsilon_{il} = (V_{ia} + V_{ii})/(V_e + V_{ia} + V_{ii})$.

We fitted the theoretical spectrum ε_{th} of this model to the measured data by using a nonlinear least square fitting algorithm based on minimisation of the variance of Eq. (10).

$$\mathrm{var} = \frac{1}{(n-1)}\sum_i^n(\varepsilon_i - \varepsilon_{thi})^2 \tag{10}$$

with n = number of measured values.

2.6. Determination of tissue water content from dielectric permittivity measurements

The effective dielectric permittivity $\varepsilon'_{w\text{-}dep}$ of water was calculated by the model displayed in Fig. 2 by replacing the dielectric permittivity $\varepsilon_e(\omega)$, $\varepsilon_{ia}(\omega)$ and $\varepsilon_{ii}(\omega)$ of the different compartments by the static dielectric permittivity $\varepsilon'_w = 78.4$ of pure water [2]. The water content was then calculated from the Maxwell–Wagner mixture formula in Eq. (11) [38] with the assumption of spherical particles with the dielectric permittivity ε'_r dissolved in the bulk with the dielectric permittivity $\varepsilon'_{w\text{-}dep}$:

$$\upsilon = \frac{\varepsilon'_{w-dep} - \varepsilon'_{heart}}{(\varepsilon'_{heart} - \varepsilon'_{w-dep})\left(\frac{\varepsilon'_{w-dep} - \varepsilon'_r}{2\varepsilon'_{w-dep} + \varepsilon'_r}\right) + 3\varepsilon'_{w-dep}\left(\frac{\varepsilon'_{w-dep} - \varepsilon'_r}{2\varepsilon'_{w-dep} + \varepsilon'_r}\right)} \tag{11}$$

with υ = volume fraction of the dissolved matter.

The dielectric permittivity ε'_{heart} was calculated from the high frequency end of the measured dielectric spectrum from 10 to 400 MHz. We fitted the theoretical spectral function of Eq. (7) extended to two Cole–Cole relaxation terms to the measured data by using the same nonlinear least square fitting algorithm. The first Cole–Cole relaxation term describes the high frequency end of the relaxation processes mentioned before, and the second Cole–Cole relaxation term describes the relaxation of the water dipole moments. For the second Cole–Cole spectral term, we used fixed parameters $\tau_w = 8.3 \times 10^{-12}$ s, $\alpha_w = 0$, and $\varepsilon_w(\infty) = 5.3$ [2]. As a result, we

obtained $\varepsilon'_{heart} = \varepsilon_w(0)$, the fitted static permittivity of the second Cole–Cole spectral term.

2.7. Statistics

The measured results are quoted as mean ± STD (standard deviation). Statistical differences between data sets were calculated by Wilcoxon rank sum test. The null hypothesis was rejected when $p \leq 0.05$.

3. Results

3.1. The complex dielectric spectrum of heart tissue during ischemia after pre-ischemic perfusion with HTK

Fig. 3 shows an example of the dielectric permittivity $\varepsilon'(\omega)$ and the conductivity $\sigma(\omega)$ of the heart at 25 °C measured at 100 and 300 min after the onset of ischemia. The spectrum is separated into segments α, β, and γ. At 100 min, ε' decreased with increasing frequency while σ increased with increasing frequency. ε' showed the high frequency end of the α-dispersion, the broad β-dispersion up to more than 100 MHz, and beyond the beginning of the γ-dispersion. Compared to this spectrum, the spectrum measured at 300 min changed as follows: The dielectric permittivity ε' was smaller in the frequency region of the α-dispersion, and higher in the beginning of the β-dispersion from 1 to about 100 kHz and a shift of the β-dispersion to higher frequencies can be seen beyond 100 kHz.

Figs. 4–7 demonstrate the time courses of $\varepsilon'(f_0)$ and $\sigma(f_0)$ during ischemia at 25 °C for hearts perfused with HTK. The observation frequencies f_0 (230 Hz, 13 kHz, 10 MHz, 354 MHz) are examples taken from the α-, beginning and high frequency end of the β-, and from the γ-region.

The dielectric permittivity ε' (230 Hz) in Fig. 4 decreased slightly during ischemia up to about 100 min and continued its decrease with a steeper negative slope up to about 250 min. Beyond this time, the dielectric permittivity was approximately constant up to 700 min. The conductivity σ (230 Hz) started with an increase up to about 60 min and decreased until 250 min. Further changes in this parameter were again negligible up to 700 min.

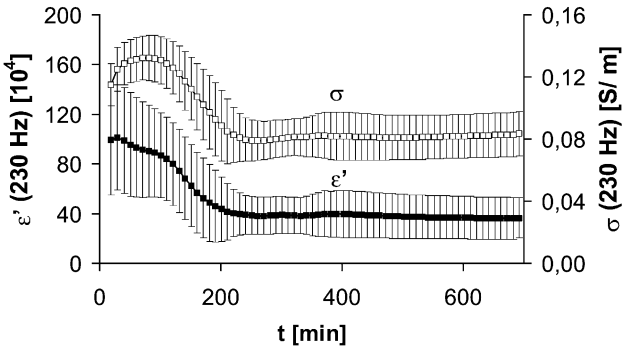

Fig. 4. Dielectric permittivity ε' and conductivity σ of heart tissue perfused with HTK measured at 230 Hz during ischemia at 25 °C (mean ± STD, $n = 6$).

The dielectric permittivity ε' (13 kHz) in Fig. 5 showed a completely different time course compared to Fig. 4. It started with a small increase, followed by a steep increase up to about 250 min and had a small maximum at about 350 min. However, the time course of the conductivity σ (13 kHz) was qualitatively similar to the time course at $f_0 = 230$ Hz.

In the higher frequency part of the β-dispersion, the time course of the dielectric permittivity as well as that of the conductivity showed a steep increase up to about 400 min, which can be seen in Fig. 6 at 10 MHz. Beyond 400 min, the rise of the increase in the dielectric permittivity ε' (10 MHz) was smaller and the conductivity σ (10 MHz) showed a plateau.

Only small changes in the dielectric permittivity ε' were measured at 354 MHz in Fig. 7. ε' (354 MHz) values between 59 and 60 can be seen during time up to about 700 min. The time course of the conductivity σ (354 MHz) showed a linear ramp up to 400 min followed by a plateau.

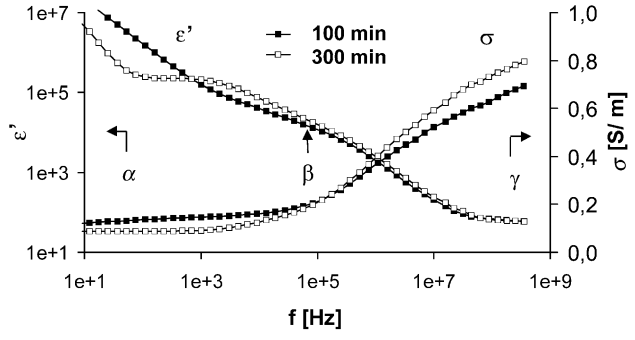

Fig. 3. Representative example of the complex dielectric permittivity spectrum of heart perfused with HTK measured at 100 and 300 min during ischemia at 25 °C.

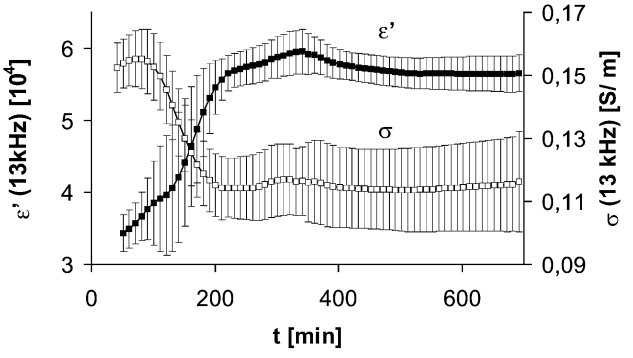

Fig. 5. Dielectric permittivity ε' and conductivity σ of heart tissue perfused with HTK measured at 13 kHz during ischemia at 25 °C (mean ± STD, $n = 6$).

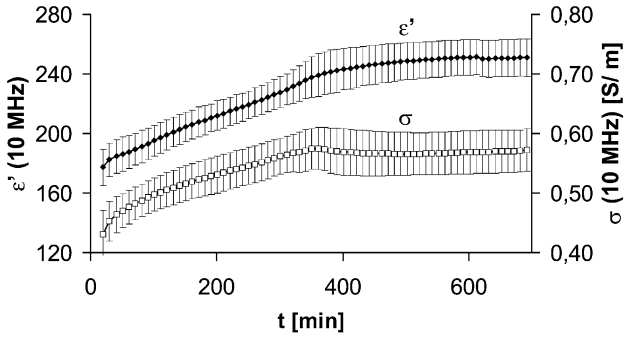

Fig. 6. Dielectric permittivity ε' and conductivity σ of heart tissue perfused with HTK measured at 10 MHz during ischemia at 25 °C (mean ± STD, $n = 5$).

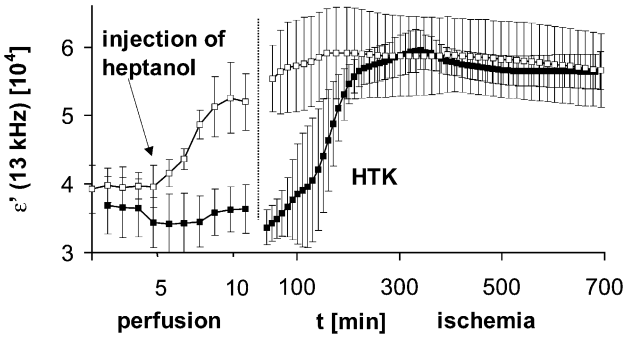

Fig. 8. Dielectric permittivity ε' of heart tissue perfused with HTK (filled symbols, $n = 6$) or with HTK + 3 mmol/l heptanol (open symbols, $n = 5$) measured at 13 kHz during perfusion and during following ischemia (mean ± STD).

3.2. The influence of heptanol perfusion on the dielectric permittivity

Fig. 8 demonstrates the different time courses of the dielectric permittivity ε' measured at 13 kHz of hearts perfused with pure HTK and HTK + heptanol, respectively. This parameter is shown during perfusion and following ischemia. During perfusion with HTK, ε' (13 kHz) ≈ 37 000 remained constant and started with similar values in the beginning of ischemia. Then followed a steep increase to values of ε' (13 kHz) ≈ 55 000 as already shown in Fig. 5. A completely different behaviour displays the time course of ε' (13 kHz) in the case of heptanol injection during perfusion: Immediately with the onset of heptanol perfusion through the heart, the dielectric permittivity increased from about 40 000 to about 53 000 and started during following ischemia with similar high values. ε' (13 kHz) of heptanol treated hearts remained beyond 50 000 during ischemia and no significant difference could be seen when compared to the dielectric permittivity values ε' (13 kHz) measured in the HTK group beyond 250 min.

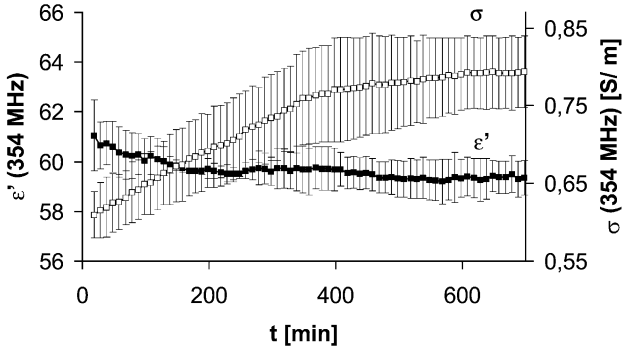

Fig. 7. Dielectric permittivity ε' and conductivity σ of heart perfused with HTK measured at 354 MHz during ischemia at 25 °C (mean ± STD, $n = 3$).

3.3. The effect of gap junction closure calculated with the equivalent circuit model of the heart

The model of Fig. 1 was used to simulate the influence of gap junction closure on the calculated dielectric permittivity spectrum. The dielectric spectrum was calculated with a small resistance R_{cc} indicating electrical cell coupling via open gap junctions, and with a very high R_{cc} for closed gap junctions. Fig. 9 demonstrates the frequency response of the calculated dielectric permittivity spectrum $\varepsilon'(\omega)$ under these different conditions. With a small resistance R_{cc}, an α- and β-dispersion appeared in $\varepsilon'(\omega)$. With increasing resistance R_{cc}, the α-dispersion disappeared and, simultaneously, ε' increased in the region of the β-dispersion. The calculated conductivity $\sigma(\omega)$ decreased with increasing R_{cc}.

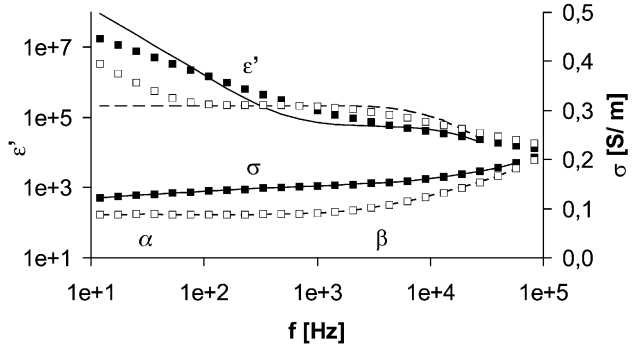

Fig. 9. Low frequency part of the spectra displayed in Fig. 3 in order to emphasise the changes during ischemia: measured complex dielectric permittivity of heart tissue at 100 min (filled symbols) and at 300 min (open symbols) in comparison to the spectra calculated with the model of Fig. 1 for open (solid line, small R_{cc}) and closed (dotted line, high R_{cc}) gap junction channels. The distribution of time constants [25–27] is not implemented in the model, which results in the differences between measured and calculated data.

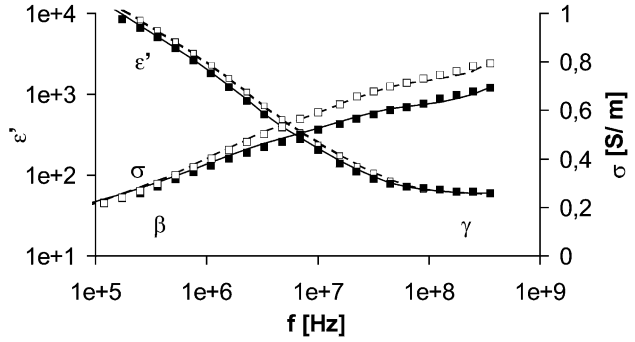

Fig. 10. High frequency part of the spectra displayed in Fig. 3 in order to emphasise the changes during ischemia: measured complex dielectric permittivity of heart tissue at 100 min (filled symbols) and at 300 min (open symbols) in comparison to the spectra (lines) calculated with the model of Fig. 2 applying the parameter sets of Table 1. Changes of the dielectric permittivity are produced by increasing model parameters σ_e, σ_{ia}, σ_{ii}, υ_{ia}, and υ_{iik}, $k=1, 2$.

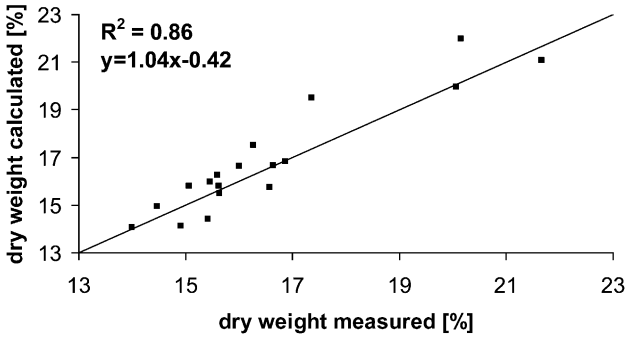

Fig. 11. Dry weight of heart tissue calculated from dielectric permittivity measurements with Maxwell–Wagner mixture formula of Eq. (11) in comparison to dry weight measured by drying and weighing the tissue.

3.4. Effect of increased conductivity, cell edema, and swelling of mitochondria on the complex dielectric permittivity spectrum

Fig. 10 shows the high frequency part of the spectra displayed in Fig. 3 in order to emphasise the changes during ischemia. It compares the dielectric spectra of the heart measured beyond 100 kHz at 100 min (filled symbols) and at 300 min (open symbols) to the fitted spectra (lines) calculated with the heart model of Fig. 2 applying the parameter sets of Table 1. As far as possible parameters were taken from literature as indicated. We kept all parameters constant except σ_e, σ_{ia}, σ_{ii}, υ_{ia} and υ_{iik}, $k=1, 2$ to fit the values at 100 and 300 min. We obtained var = 38 at 100 min and var = 150 at 300 min, respectively.

3.5. The dielectric permittivity and the water content of heart tissue

An effective dielectric permittivity $\varepsilon'_{w\text{-}dep}=76$ of water was determined with the model of Fig. 2 applying the parameters of Table 1 describing the cell morphology. The volume fraction of the nonpolar component with $\varepsilon'_r=3$ was calculated from Eq. (11) for each heart with the dielectric permittivity ε'_{heart}. Fig. 11 compares these results with the

Table 1
Parameter sets for the calculation of the complex dielectric spectrum of the heart with the model of Fig. 2

Parameter	100 min	300 min	Comparison to literature
Dielectric properties			
ε_e, $\varepsilon_e(\infty)$, τ_e [ps], α_e, σ_e [S/m]	82, 5, 9, 0, **1.29** (1.31 ± 0.04)	82, 5, 9, 0, **1.37** (1.52 ± 0.24)	perfusion solution—measured
ε_{ia}, $\varepsilon_{ia}(\infty)$, τ_{ia} [ps], α_{ia}, σ_{ia} [S/m]	50, 5, 30, 0, **0.47** (0.61 ± 0.16)	50, 5, 30, 0, **0.69** (0.69 ± 0.07)	$50 \le \varepsilon_{ia} \le 80$ [36], $0.1 \le \sigma_{ia} \le 1.0$ [46]
ε_{ii}, $\varepsilon_{ii}(\infty)$, τ_{ii} [ps], α_{ii}, σ_{ii} [S/m]	25, 3, 40, 0, **0.34** (0.25 ± 0.08)	25, 3, 40, 0, **0.41** (0.27 ± 0.1)	–
ε_m, $\varepsilon_m(\infty)$, τ_m [ps], α_m, σ_m [S/m]	8, 3, 1×10^7, 0.3, 9×10^{-7}	8, 3, 1×10^7, 0.3, 9×10^{-7}	$\varepsilon_m \approx 3$ [46]
ε_{mi}, $\varepsilon_{mi}(\infty)$, τ_{mi} [ps], α_{mi}, σ_{mi} [S/m]	3, 3, 2×10^{10}, 0, 9×10^{-7}	3, 3, 2×10^{10}, 0, 9×10^{-7}	$\varepsilon_{mi} \approx 3$ [46]
Cell morphology			
Ellipsoid half axis of the cells, $a, b=c$ [μm]	60, 10	60, 10	[47]
Cell membrane thickness, d_m [m]	25×10^{-10}	25×10^{-10}	$10\times10^{-10} \le d_m \le 40\times10^{-10}$ [42,48]
Cellular volume fraction, υ_{ia}	**0.61** (0.63 ± 0.04)	**0.63** (0.65 ± 0.04)	$0.65 \le \upsilon_{ia} \le 0.85$ [42,43]
Intracellular structures			
Ellipsoid half axis of the cells, $a_1, b_1=c_1$ [μm]	1.5, 0.3	1.5, 0.3	$0.5 \le \varnothing \le 6$ μm [49]
Membrane thickness, d_{mi1} [m]	50×10^{-10}	50×10^{-10}	–
Volume fraction, υ_{ii1}	**0.37** (0.32 ± 0.05)	**0.39** (0.36 ± 0.04)	0.36 [47]
Ellipsoid half axis of the cells, $a_2, b_2=c_2$ [μm]	3, 3	3, 3	$0.5 \le \varnothing \le 6$ μm [49]
Volume fraction, υ_{ii2}	**0.129** (0.11 ± 0.06)	**0.131** (0.12 ± 0.06)	–
Membrane thickness, d_{mi2} [m]	25×10^{-10}	25×10^{-10}	–

Parameters given with plain characters are taken from literature as indicated. Bold parameters describing the changes between 100 and 300 min were obtained by nonlinear least squares fit from the data shown in Fig. 10. Data in brackets following the bold parameters are mean ± STD calculated by fitting different experimental data in order to show parameter variation in different hearts ($n=3$).

results obtained by drying and weighing the heart samples. A correlation factor of $R^2 = 0.86$ was found.

4. Discussion

4.1. Influence of gap junction closure on the complex dielectric spectrum of heart tissue between 10 Hz and 100 kHz

The application of heptanol closes gap junctions definitely which was shown by patch-clamp investigations on paired cells [29]. During perfusion, the dielectric permittivity ε' (13 kHz) in Fig. 8 increases immediately to values beyond 50 000 after addition of heptanol to the perfusion solution and remains constant during following ischemia. In the case of hearts perfused with HTK solution without heptanol, a similar increase in ε' (13 kHz) beyond 50 000 was found only after 250 min of ischemia at 25 °C. An intraischemic closure of gap junctions could be the cause of this increase. Although we have no independent evidence for this interpretation, the simulations of the gap junction closure with the model of Fig. 1 support this presumption. Fig. 9 shows three simultaneous changes in the dielectric permittivity spectrum: a decrease of $\varepsilon'(\omega)$ in the α-region, an increase of $\varepsilon'(\omega)$ in the β-region, and an overall decrease of $\sigma(\omega)$. A steep decrease of ε' in the α-region is observed beyond about 100 min up to 250 min in the time course of ε' (230 Hz) in Fig. 4. A parallel increase of ε' and a decrease of σ in the β-region is found in the time course at 13 kHz in Fig. 5. Hence, the measurements behave exactly as predicted by the model. From this we conclude that these changes in the complex dielectric permittivity spectrum in the frequency range from 10 Hz to 100 kHz are produced by the closure of gap junctions.

The variation of the membrane resistance also affects the complex dielectric permittivity spectrum in this frequency range [21,39]. If we simulate an increase of R_m with our model keeping all other parameters constant, this leads also to a decrease of the conductivity σ at frequencies below 50 kHz. However, in contrast to the measured results between 100 and 250 min in Fig. 4, the dielectric permittivity ε' is increased in the frequency region of the α-dispersion. Therefore, within the scope of the model of Fig. 1, an increase of the membrane resistance R_m does not explain the measured changes of ε' (230 Hz), ε' (13 kHz), and σ (13 kHz) in this time interval. This shows that the analysis of only one parameter (e.g. σ) is not sufficient to identify gap junction closure.

Now we can answer question (1) formulated in the introduction: The theoretical investigations performed with the heart model, as well as the experiments with heptanol, support the presumption that the physical process of gap junction closure can be detected in the complex dielectric spectrum of the heart by the parallel analysis in the α- and β- region.

4.2. Influence of cell orientation, conductivity, and intracellular volume fraction on the complex dielectric spectrum between 100 kHz and 400 MHz of heart tissue during ischemia

Within the scope of the model of Fig. 2, we obtain a reasonably good fit to the measured data as shown in Fig. 10, although we assume arbitrarily oriented cell ellipsoids and arbitrarily oriented ellipsoids for intracellular structures. However, from anatomy, it is well known that heart cells in the ventricular walls are oriented in layers. We assume that the inhomogeneous electric fields used for the measurements are responsible for this result because the curved electrical field lines penetrate the heart cells in various directions. In relation to the measuring system, the cells appear arbitrarily oriented.

Metabolic measurements reveal the intraischemic production of ions, which increases the specific conductivity [40]. A developing cell edema and the swelling of mitochondria during ischemia is known from histology [41]. These processes are modelled by the parameters σ_e, σ_{ia}, σ_{ii}, υ_{ia}, υ_{ii1}, and υ_{ii2}, respectively. Parameters σ_j, $j = e$, ia, ii describe the specific conductivity of the extra- and intracellular compartments. Between 100 and 300 min, these values increase from 1.29 to 1.37, 0.47 to 0.69, and 0.34 to 0.41, respectively (cf. Table 1). Parameter υ_{ia}, which models the cellular volume fraction, increases from 0.61 to 0.63. In our model, we distinguish only two intracellular structures with membranes described by their volume fraction υ_{ii1} and υ_{ii2}. These values also increase between 100 and 300 min from 0.37 to 0.39 and 0.129 to 0.131, respectively.

Absolute values of the calculated model parameters strongly depend on the additional input parameters describing the different ellipsoids and the complex dielectric properties of the model compartments (cf. Table 1). Some of these parameters are not exactly known, especially not under the condition of ischemia. We varied some of these parameters in physically reasonable ranges yielding different fit results. However, for each parameter set we tested, σ_e, σ_{ia}, σ_{ii}, υ_{ia}, υ_{ii1}, and υ_{ii2} increased from 100 to 300 min as described above for the single experiment. In order to show the robustness of our model approach, we applied the parameter set of Table 1 to different experiments of the same experimental group and finally calculated mean and STD for each fit parameter (data are shown in brackets in Table 1). For these data, we did not find a large variation.

Answering question (2) of the introduction, the changes of the model parameters calculated by fitting the example in Fig. 10 at 100 and 300 min match the results of the abovementioned metabolic and histologic investigations during ischemia.

4.3. The influence of the cell shape and the shape of intracellular structures on the dielectric permittivity

To calculate the water content of the heart tissue, we used the Maxwell mixture formula of Eq. (11). This formula is based on the tissue model of spherical particles with the dielectric permittivity ε'_r dissolved in a bulk medium of water with the dielectric permittivity of ε'_w. The main polarisation contribution to the dielectric permittivity of biological tissue beyond several hundred MHz is due to the molecular dipole moments of water [5,34]. The dielectric permittivity of pure water at 25 °C amounts to $\varepsilon'_w = 78.4$ in this frequency range [2]. The nonaqueous part of the tissue matter is beyond its relaxation frequency and shows small dielectric permittivity values of typically $\varepsilon'_r = 3-5$.

Water is found in the intra- and extracellular compartment. The cellular volume fraction is between 0.65 and 0.85 [42,43], and the largest amount of water molecules can be found inside the cells. Hence, to apply the Maxwell mixture formula we have to decrease the dielectric permittivity from $\varepsilon'_w = 78.4$ to $\varepsilon'_{w\text{-}dep} = 76$ to allow for the depolarising electrical field from the cell membranes [28]. $\varepsilon'_{w\text{-}dep}$ was calculated with the heart model of Fig. 2 as described in Materials and methods.

In order to determine the dielectric permittivity ε'_{heart} in Eq. (11), we used a Cole–Cole spectral function with parameters τ_w and α_w found for pure water [2]. This means, all tissue water is assumed to be in free form as found for skeletal muscle [44] and effects of bound water [45] are neglected.

We compared the dry weight calculated with the mixture formula to the water content independently gained by drying and weighing the heart tissue (cf. Fig. 11) and found a good correlation between the values. The average absolute difference is 0.7 using $\varepsilon'_{w\text{-}dep}$ and 2.3 using ε'_w in the Maxwell mixture formula. Hence, as an answer to question (3) of the introduction, we conclude that within the scope of our model the depolarisation of cell membranes and membranes of intracellular structures must be taken into account to determine the tissue water content.

4.4. Assessment of intraischemic heart tissue damage by dielectric spectroscopy

It was already suggested by Gebhard [13] and Ischikawa [16] to use the passive electrical properties of the heart for the assessment of tissue damage during ischemia. They tried to correlate changes in the passive electrical properties to information gained by biochemical and histological investigations.

In this paper, we try to link intraischemic processes to changes in the dielectric spectrum of the heart. By using appropriate models to describe the dielectric properties of heart tissue, we can extract the following tissue parameters from the measured data: (1) tissue water content, (2) volume fraction of cells and of intracellular structures in the tissue, (3) conductivity of the extra- and intracellular compartments, and (4) intercellular coupling via gap junctions. The influence of these tissue parameters for functional recovery of the heart after resuscitation is only partially understood. The intraischemic swelling of cells or of mitochondria [41] is an indicator for tissue damage. Intercellular uncoupling via gap junction closure is discussed to be a reason for certain heart diseases as for example arrhythmia [21] or hibernation [20]. The closure of gap junctions accompanied by other intraischemic alterations like a decrease of ATP below a critical threshold [40] could be a signal for evolving organ damage [14]. However, intercellular uncoupling was found to be reversible under specific ischemic conditions [18].

Ischemic heart tissue finally perishes due to many cellular and intracellular processes some of which can be noninvasively monitored by dielectric spectroscopy. The next step will be to find a critical range for the transition from reversible to irreversible tissue damage by a more detailed analysis of the time course of dielectric parameters.

Acknowledgements

We would like to thank Prof. Dr. Reinhard Pottel for many helpful discussions on tissue modelling.

References

[1] J.R. Macdonald, Impedance Spectroscopy, Wiley, New York, 1987.
[2] U. Kaatze, V. Uhlendorf, Dielectric properties of water at microwave frequencies, Z. Phys. Chem. 126 (1981) 152–165.
[3] C. Grosse, M. Tirado, W. Pieper, R. Pottel, Broad frequency range study of dielectric suspensions of colloidal polystyrene particles in aqueous electrolyte solutions, J. Colloid Interface Sci. 205 (1998) 26–41.
[4] H.P. Schwan, Electrical properties of tissues and cell suspensions, Adv. Biol. Med. Phys. 5 (1957) 147–209.
[5] K.R. Foster, H.P. Schwan, Dielectric properties of tissues and biological materials: a critical review, Crit. Rev. Biomed. Eng. 17 (1989) 25–104.
[6] B. Rigaud, J.-P. Morucci, N. Chauveau, Bioelectrical impedance techniques in medicine, Crit. Rev. Biomed. Eng. 24 (1996) 257–351.
[7] K. Asami, A. Irimajiri, T. Hanai, N. Shiraishi, K. Utsumi, Dielectric analysis of mitochondria isolated from rat liver: I. Swollen mitoplasts as stimulated by a single shell model, Biochim. Biophys. Acta 778 (1984) 559–569.
[8] K. Asami, A. Irimajiri, Dielectric analysis of mitochondria isolated from rat liver: II. Intact mitochondria as simulated by a double-shell model, Biochim. Biophys. Acta 778 (1984) 570–578.
[9] V. Raicu, T. Saibara, A. Irimajiri, Multifrequency method for dielectric monitoring of cold-preserved organs, Phys. Med. Biol. 45 (2000) 1397–1407.
[10] M. Schäfer, H.J. Kirlum, C. Schlegel, M.M. Gebhard, Dielectric properties of skeletal muscle during ischemia in the frequency range from 50 Hz to 200 MHz, Ann. N.Y. Acad. Sci. 873 (1999) 59–64.
[11] T. Oltrup, T. Bende, K.D. Kramer, B. Jean, Dielectric spectroscopy for noninvasive examination of corneal tissue, Biomed. Tech. 44 (2001) 78–82.
[12] S. Gabriel, R.W. Lau, C. Gabriel, The dielectric properties of biological tissues: II. Measurements in the frequency range 10 Hz to 20 GHz, Phys. Med. Biol. 41 (1996) 2251–2269.

[13] M.M. Gebhard, E. Gersing, C.J. Brockhoff, Ph.A. Schnabel, H.J. Bretschneider, Impedance spectroscopy: a method for surveillance of ischemia tolerance of the heart, Thorac. Cardiovasc. Surg. 35 (1987) 26–32.
[14] E. Gersing, Impedance spectroscopy on living tissues for determination of the organ state, Bioelectrochem. Bioenerg. 45 (1998) 145–149.
[15] O. Casas, R. Bragos, P.J. Riu, J. Rosell, M. Tresanchez, M. Warren, A. Rodriguez-Sinovas, A. Carreno, J. Cinca, In vivo and in situ ischemic tissue characterization using electrical impedance spectroscopy, Ann. N.Y. Acad. Sci. 873 (1999) 51–58.
[16] M. Ishikawa, H. Hirose, E. Sasaki, M. Bando, Y. Mori, S. Murakawa, Evaluation of myocardial viability during simple cold storage with the use of electrical properties in broad frequencies, J. Heart Lung Transplant. 15 (1996) 1005–1011.
[17] L.M. Owens, T.A. Fralix, E. Murphy, W.E. Cascio, L.S. Gettes, Correlation of ischemia-induced extracellular and intracellular ion changes to cell-to-cell electrical uncoupling in isolated blood-perfused rabbit hearts, Circulation 94 (1996) 10–13.
[18] M.A. Beardslee, D.L. Lerner, P.N. Tadros, J.G. Laing, E.C. Beyer, K.A. Yamada, A.G. Kleber, R.B. Schuessler, J.E. Saffitz, Dephosphorylation and intracellular redistribution of ventricular connexin43 during electrical uncoupling induced by ischemia, Circ. Res. 87 (2000) 656–662.
[19] M. Schäfer, E. Gersing, M.M. Gebhard, Characterization of organ tissue during the transition between life and death: cardiac and skeletal muscle, Med. Biol. Eng. Comput. 37 (1999) 100–101.
[20] J.E. Saffitz, K.A. Yamada, Do alterations in intercellular coupling play a role in cardiac contractile dysfunction? Circulation 97 (1998) 630–632.
[21] E. Carmeliet, Cardiac ionic currents and acute ischemia: from channels to arrhythmias, Physiol. Rev. 79 (1999) 917–1017.
[22] P. Daleau, S. Boudriau, M. Michaud, C. Jolicoeur, J.G. Kingma Jr., Preconditioning in the absence or presence of sustained ischemia modulates myocardial Cx43 protein levels and gap junction distribution, Can. J. Physiol. Pharm. 79 (2001) 371–378.
[23] J.R. de Groot, F.J. Wilms-Schopman, T. Opthof, C.A. Remme, R. Coronel, Late ventricular arrhythmias during acute regional ischemia in the isolated blood perfused pig heart. Role of electrical cellular coupling, Cardiovasc. Res. 50 (2001) 362–372.
[24] S. Dhein, Cardiac Gap Junctions, Karger, Basel, 1998.
[25] M. Gheorghiu, E. Gersing, E. Gheorghiu, Quantitative analysis of impedance spectra of organs during ischemia, Ann. N.Y. Acad. Sci. 873 (1999) 65–71.
[26] V. Raicu, Dielectric dispersion of biological matter: model combining Debye-type and "universal" responses, Phys. Rev., E 60 (1999) 4677–4680.
[27] K.S. Paulson, S. Jouravleva, C.N. McLeod, Dielectric relaxation time spectroscopy, IEEE Trans. Biomed. Eng. 47 (2000) 1510–1517.
[28] R. Pottel, D. Göpel, R. Henze, U. Kaatze, V. Uhlendorf, The dielectric permittivity spectrum of aqueous colloidal phospholipid solutions between 1 kHz and 60 GHz, Biophys. Chemist. 19 (1984) 233–244.
[29] B.R. Takens-Kwak, H.J. Jongsma, M.B. Rook, A.C. Van Ginneken, Mechanism of heptanol-induced uncoupling of cardiac gap junctions: a perforated patch-clamp study, Am. J. Physiol. 262 (1992) C1531–C1538.
[30] M. Schäfer, C. Schlegel, H.J. Kirlum, M.M. Gebhard, Monitoring of damage to skeletal muscle tissues caused by ischemia, Bioelectrochemistry 45 (1998) 151–155.
[31] E. Gersing, Measuring electrical impedance of organs-instrumental equipment for research and clinical use, Biomed. Tech. 36 (1991) 6–11.
[32] E. Meyer, R. Pottel, Physikalische Grundlagen der Hochfrequenztechnik, Vieweg & Sohn, Braunschweig, 1969.
[33] D. Misra, A quasi-static analysis of open-ended coaxial lines, IEEE Trans. MTT 35 (1987) 925–928.
[34] R. Pethig, Dielectric properties of body tissues, Clin. Phys. Physiol. Meas. 8 (Suppl. A) (1987) 5–12.
[35] C.J.F. Böttcher, P. Bordeweijk, Theory of Electric Polarisation, Elsevier, Amsterdam, 1978.
[36] K. Asami, T. Hanai, N. Koizumi, Dielectric approach to suspensions of ellipsoidal particles covered with a shell in particular reference to biological cells, Jap. J. Appl. Phys. 19 (1980) 359–365.
[37] D. Polder, J.H. Van Santen, The effective permeability of mixtures of solids, Physica 12 (1946) 257–271.
[38] Y. Polevaya, I. Ermolina, M. Schlesinger, B.Z. Ginzburg, Y. Feldman, Time domain dielectric spectroscopy study of human cells: II. Normal and malignant white blood cells, Biochim. Biophys. Acta 1419 (1999) 257–271.
[39] S. Despa, The influence of membrane permeability for ions on cell behaviour in an electric alternating field, Phys. Med. Biol. 40 (1995) 1399–1409.
[40] M.M. Gebhard, H.J. Bretschneider, P.A. Schnabel, Cardioplegic principles and problems, in: N. Sperelakis (Ed.), Physiology and Pathophysiology of the Heart, Kluwer Academic Publishing, Boston, 1989, pp. 655–669.
[41] P.A. Schnabel, M.M. Gebhard, T. Pomykaj, A. Schmiedl, C.J. Preusse, J. Richter, H.J. Bretschneider, Myocardial protection: left ventricular ultrastructure after different forms of cardiac arrest, Thorac. Cardiovasc. Surg. 35 (1987) 148–156.
[42] P.A. Poole-Wilson, I.R. Cameron, ECS, intracellular pH, and electrolytes of cardiac and skeletal muscle, Am. J. Physiol. 229 (1975) 1299–1304.
[43] Q.R. Smith, L.K. Pershing, C.E. Johanson, A comparative analysis of extracellular fluid volume of several tissues as determined by six different markers, Life Sci. 29 (1981) 449–456.
[44] M.A. Stuchly, A. Kraszewski, S.S. Stuchly, A.M. Smith, Dielectric properties of animal tissues in vivo at radio and microwave frequencies: comparison between species, Phys. Med. Biol. 27 (1982) 927–936.
[45] E.H. Grant, The dielectric method of investigating bound water in biological material: an appraisal of the technique, Bioelectromagnetics 3 (1982) 17–24.
[46] T. Hanai, N. Koizumi, A. Irimajiri, A method for determining the dielectric constant and the conductivity of membrane-bounded particles of biological relevance, Biophys. Struct. Mech. 1 (1975) 285–294.
[47] A.M. Katz, Physiology of the Heart, Raven Press, New York, 1992.
[48] N.M. Rao, A.L. Plant, V. Silin, S. Wight, S.W. Hui, Characterization of biomimetic surfaces formed from cell membranes, Biophys. J. 73 (1997) 3066–3077.
[49] W. Hoppe, W. Lohmann, H. Markl, H. Ziegler, Biophysik, Springer, Berlin, 1982.